MOTIF-BASED GRAPH REPRESENTATION LEARNING WITH APPLICATION TO CHEMICAL MOLECULES

Anonymous authors
Paper under double-blind review

ABSTRACT

This work considers the task of representation learning on the attributed relational graph (ARG). Both the nodes and edges in an ARG are associated with attributes/features allowing ARGs to encode rich structural information widely observed in real applications. Existing graph neural networks offer limited ability to capture complex interactions within local structural contexts, which hinders them from taking advantage of the expression power of ARGs. We propose **M**otif **C**onvolution **M**odule (MCM), a new motif-based graph representation learning technique to better utilize local structural information. The ability to handle continuous edge and node features is one of MCM's advantages over existing motif-based models. MCM builds a motif vocabulary in an unsupervised way and deploys a novel motif convolution operation to extract the local structural context of individual nodes, which is then used to learn higher-level node representations via multilayer perceptron and/or message passing in graph neural networks. When compared with other graph learning approaches to classifying synthetic graphs, our approach is substantially better in capturing structural context. We also demonstrate the performance and explainability advantages of our approach by applying it to several molecular benchmarks.

1 INTRODUCTION

The amount of graph data has grown explosively across disciplines (e.g., chemistry, social science, transportation, etc.), calling for robust learning techniques for modeling knowledge embedded in graphs and performing inference on new graphs. To shed new light on the mechanisms underlying observations, the learning techniques need to be interpretable so that we can link structural patterns to properties of interest. Many types of complex graphs (e.g., chemical molecules, biological molecules, signal transduction networks, multi-agent systems, social networks, knowledge graphs, etc.) can be naturally represented as attributed relational graphs (ARGs) Barrow & Popplestone (1971); Tsai & Fu (1979). The ARG representation extends ordinary graph representations by associating attributes (or features) with nodes and edges to characterize the corresponding entities and relationships, respectively. This makes ARGs substantially more expressive, which makes them appealing to many real-world applications, however, the nuance of ARGs comes with added complexities in training and analysis. We denote an ARG as $G =< \{v\}, \{e_{uv}\}, \{\mathbf{a}_v\}, \{\mathbf{r}_{u,v}\} >$, where $\{v\}$ is the node set, $\{e_{u,v}\}$ is the relation set with $e_{u,v}$ indicating the relation between nodes u and v, and $\mathbf{a}_v$ and $\mathbf{r}_{u,v}$ are the attribute vectors of node v and relationship $e_{u,v}$, respectively.

Recently, graph neural networks (GNNs) Baskin et al. (1997); Sperduti & Starita (1997); Gori et al. (2005); Scarselli et al. (2005), which operate on the graph domain, have been combined with deep learning (DL) LeCun et al. (2015) to take advantage of big graph data. Many GNN variants have been proposed for a variety of applications (e.g., visual scene understanding, learning dynamics of physical systems, predicting properties of molecules, predicting traffic, etc.) Bruna et al. (2014); Henaff et al. (2015); Duvenaud et al. (2015); Defferrard et al. (2016); Li et al. (2016); Monti et al. (2017); Chang et al. (2017); Gilmer et al. (2017a); Chang et al. (2018); Velickovic et al. (2018); Xu et al. (2018a). In this study, we focus on the application of graph representation learning to efficiently and accurately estimate the properties of chemical molecules, which is in high demand to accelerate the discovery and design of new molecules/materials. In addition, there is an abundance of publicly available data in this domain, for example, the QM9 dataset Ramakrishnan et al. (2014). In the QM9 dataset, each chemical molecule is represented as an ARG with nodes and relations representing atoms and bonds, respectively. Each node has one attribute storing the atom ID and the 3D coordinates, and each relation has attributes indicating bond type (single/double/triple/aromatic) and length.

Accurate quantum chemical calculation (e.g., typically using density functional theory (DFT)) needs to consider complex interactions among atoms and requires a prohibitively large amount of computational resources, preventing the efficient exploration of vast chemical space. There have been increasing efforts to overcome this bottleneck using GNN variants to approximate DFT simulation, such as, enn-s2s Gilmer et al. (2017b), SchNet Schütt et al. (2017), MGCN Lu et al. (2019), DimeNet Klicpera et al. (2020b), DimeNet++ Klicpera et al. (2020a), and MXMNet Zhang et al. (2020).

GNNs aim to learn embeddings (or representations) of nodes and relations to capture complex interactions within graphs, which can be used in downstream tasks, such as graph property prediction, graph classification, and so on. The message passing mechanism is widely used by GNNs to approximate complex interactions. A GNN layer updates the embedding of a node v by transforming messages aggregated from its neighbors:

$$\mathbf{a}_v^{(l+1)} = f_1(\mathbf{a}_v^{(l)}, \sum_{u \in \mathcal{N}_v} f_2(\mathbf{a}_u^{(l)}, \mathbf{r}_{uv}^{(l)})) \tag{1}$$

where l indicates the l-th GNN layer ($l = 0$ corresponds to the input), $\mathcal{N}_v$ is the neighbor set of node v, $\mathbf{a}_v^{(l)}$ is the embedding of node v, $\mathbf{r}_{uv}^{(l)}$ is the embedding of relation e_{uv}, f_1 is the node embedding update function, and f_2 is the interaction function passing messages from neighbors. The functions f_1 and f_2 can be based on neural networks. Relation embedding update can also be implemented using neural networks to integrate the l-th layer embedding of a relation with the l- or $(l+1)$-th layer embeddings of the nodes connected to the relation.

In the context of predicting molecular properties, innovations in GNN variants mainly focus on improving message-passing to better utilize structural information. For example, SchNet Schütt et al. (2017) considers the lengths of relationships (i.e., bonds between atoms) using a band of radial basis functions when calculating message-passing. MGCN Lu et al. (2019) stacks GNN layers to hierarchically consider quantum interaction at the levels of individual atoms, atom pairs, atom triads, and so on. When calculating the message passing to a target node from one of its neighbors, DimeNet Klicpera et al. (2020b) proposes directional embedding to capture interactions between neighboring bond pairs and is invariant in rotation and translation. DimeNet++ Klicpera et al. (2020a) improves the efficiency of DimeNet by adjusting the number of embedding layers and the embedding sizes via down-/up-projection layers. MXMNet Zhang et al. (2020) analyzes the complexity of the directional embedding proposed in DimeNet and decomposes molecule property calculations into local and non-local interactions, which can be modeled by local and global graph layers, respectively. The expensive directional embedding is only used in the local graph layer. In addition, MXMNet proposes efficient message passing methods to approximate interaction up to two-hop neighbors in the global layer and interactions up to two-hop angles in the local graph layer.

Existing GNNs typically start with node attributes, which do not efficiently capture structural information. In addition, each message passing calculation considers limited local context of the destination node. Most of the early studies on GNNs treated relations as independent in each iteration of message calculation. DimeNet/DimeNet++ and MXMNet consider the interaction between a 1-hop relation and its neighboring 2-hop relations. Although MGCN can potentially add higher layers to directly consider larger local contexts, its interaction space will increase exponentially with respect to the layer number. Moreover, it may not be straightforward to choose the number of levels because nodes have different local context sizes. We hypothesize that the local context space can be well characterized by a set of motifs, each of which may correspond to a certain type of local structure/substructure. For example, a motif may represent a chemical functional group. The motif set can be learned from data and be used to extract node features that explicitly encode the local context of the corresponding node, and hence improve the performance of a GNN. We, therefore, propose a motif-based graph representation learning approach with the following major components: (a) unsupervised pre-training of motifs; (b) motif convolution for isomorphic invariant and local-structure-aware embedding; (c) highly explainable motif-based node embeddings; and (d) a GPU-enabled motif convolution implementation to overcome the high computational complexity. We demonstrate our approach by its application to both synthetic and chemical datasets.

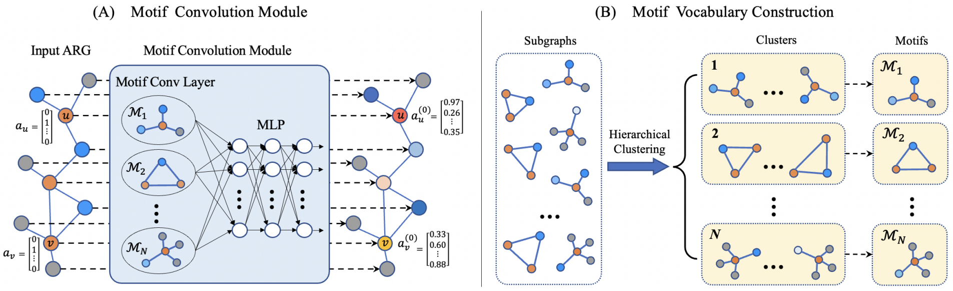

Figure 1: Motif Convolution Module. (A) The convolution operation calculates the structural similarity score between every of the N motifs and the subgraph centering at each node in the input graph (see Sections 2.2 and 2.3) to produce a N-dimension context-aware representation for the corresponding node, which is further transformed by a multilayer perceptron (MLP) network to produce a MCM-embedding for the input node. For example, although two input nodes u and v represent the same element (e.g., atom), their MCM-embeddings $a_u^{(0)}$ and $a_v^{(0)}$ are different as u and v are in different local context. An expanded illustration of MCM is shown in Figure A.6 in Appendix. The output of MCM can be fed into GNNs. (B) The motif vocabulary is built via clustering on subgraphs sampled from input graphs (Section 2.1).

2 Motif-based Graph Representation Learning

The key of our motif-based representation learning technique is a motif convolution module (MCM) (Figure 1A), which contains a motif convolution layer (MCL) connected to an optional multilayer perceptron (MLP) network. The motifs in an MCL are spatial patterns and can be constructed by clustering subgraphs extracted from training graphs (Figure 1B). These motifs describe various substructures representing different local spatial contexts. The convolution step applies all motifs on every node in an input graph to produce a local-context-aware node representation, which is invariant to transformations (rotation and translation in 3D). The MLP component can further embed the above node representation by exploring interactions between motifs. The node embeddings produced by MCM encode local structural context, which can empower downstream computations to learn richer semantic information. Below we explain in more details about motif vocabulary construction, motif convolution, and using MCM with GNNs.

2.1 Motif vocabulary construction

Ideally, the motif vocabulary should be learned in an end-to-end fashion; however, this would incur an extremely high computational complexity. Therefore, we turned to a straightforward method for building a motif vocabulary that represents recurrent spatial patterns in training ARGs. First, we sampled a large number of subgraphs (e.g., k-hop neighborhoods) from the dataset. Each subgraph records its own center node. To make the extracted subgraphs cover local contexts as much as possible, we reduced the probability of sampling a subgraph by 50% if the center node of the subgraph already appears in a sampled subgraph. This allows unvisited local contexts to be sampled with greater probability. Highly similar subgraphs (up to 3D rotation+translation transformations) can be represented by one motif. To achieve this, the sampled subgraphs are grouped into a user-specified number of clusters using a hierarchical clustering technique using average linkage Johnson (1967), implemented in the Orange3 library Demšar et al. (2013). A representative subgraph is selected from each cluster as a motif. If the size of the whole subgraph set is too big for the hierarchical clustering algorithm, we can randomly partition the whole subgraph set into many smaller subsets, and apply the above procedure to extract representative subgraphs from each subset. The above procedure is then applied to the representative subgraphs extracted from all subsets to obtain the final motifs. Pair-wise similarity calculations are required to perform hierarchical clustering between subgraphs (each of which are ARGs).

2.2 ARG similarity measurement

We need to measure the similarity between two ARGs when building the motif vocabulary (Section 2.1) and performing motif convolutions (Section 2.3). Such a similarity measurement should be invariant to the permutation of nodes, which requires node-to-node matching between two graphs. In addition, the similarity measurement should not be sensitive to graph sizes. Otherwise, a larger graph could have a higher chance to be more similar to a motif than a smaller graph. Assuming we have the node-to-node matching, which is represented by a matching matrix $\mathbf{M}$, between two ARGs G_1 and G_2. Each element $\mathbf{M}_{ui} \in \{0, 1\}$ indicates whether node u in G_1 matches with node i in G_2. Inspired by Gold & Rangarajan (1996); Menke & Yang (2020), we define the normalized similarity between G_1 and G_2 defined as:

$$S(G_1, G_2) = (\sum_{u=1}^{n_1}\sum_{i=1}^{n_2}\sum_{v=1}^{n_1}\sum_{j=1}^{n_2} \frac{\mathbf{M}_{ui}\mathbf{M}_{vj}s_1(e_{uv}^{(1)}, e_{ij}^{(2)})}{2\sqrt{l_1 \times l_2}} + \alpha \frac{\sum_{u=1}^{n_1}\sum_{i=1}^{n_2}\mathbf{M}_{ui}s_2(u,i)}{\sqrt{n_1 \times n_2}}) \times \frac{1}{1+\alpha} \tag{2}$$

where n_1 and n_2 are the numbers of nodes in G_1 and G_2, respectively. l_1 and l_2 are the numbers of edges in G_1 and G_2, respectively, $s_1(e_{uv}^{(1)}, e_{ij}^{(2)})$ is the relation compatibility function measuring the similarity between $e_{uv}^{(1)} \in G_1$ and $e_{ij}^{(2)} \in G_2$, $s_2(u, i)$ is the node compatibility function measuring the similarity between node $u \in G_1$ and node $i \in G_2$. α is the trade-off parameter to balance the contributions from edge similarities and node similarities. Theorem 2.1 shows that $S(G_1, G_2)$ is independent of graph sizes. A matching matrix $\mathbf{M}$ is required to compute $S(G_1, G_2)$. Finding an optimal matching between two ARGs is an NP problem and has been widely studied. We leave the details of problem definition and the efficient algorithm for finding a sub-optimal $\mathbf{M}$ in Appendix A.3. We have developed a GPU-accelerated matching method with sublinear complexity (see discussions in Appendix A.3.5).

Theorem 2.1 *If the compatibility functions $s_1(e_{uv}^{(1)}, e_{ij}^{(2)})$ and $s_2(u, i)$ are well-defined and normalized compatibility metrics, $S(G_1, G_2)$ achieves maximum of 1 if and only if G_1 and G_2 are isomorphic. [proof in Appendix A.2]*

2.3 MOTIF CONVOLUTION

The motif convolution layer (MCL) computes the similarity (see Section 2.2) between every motif and the subgraph centered at each node in an input graph. A motif representation of each input node is obtained by concatenating the similarity scores between the subgraph of the node and all motifs. This representation can be fed into a trainable multi-layer perceptron (MLP) with non-linear activation functions (e.g., ReLU) to produce a further embedding that encodes interactions among motif features. We denote this operation as:

$$\mathbf{a}_u^{(0)} = \text{MCM}(u \in G; \{\mathcal{M}_i\}_{i=0}^{N})) \tag{3}$$

where G is an input ARG, u is a node in G, $\{\mathcal{M}_i\}_{i=0}^{N}$ represents the motif vocabulary of size N, and $\mathbf{a}_u^{(0)}$ is the MCM-embedding of u. Figure A.6 in Appendix shows an expanded illustration of the MCM computation flow.

2.4 COUPLING MOTIF CONVOLUTION WITH GNNS

The MCM can serve as a preceding module for any GNN to form MCM+GNN. The output of the MCM is still an ARG, which can be fed into any GNN that accepts an ARG as input. A readout function of an MCM+GNN model is needed to obtain the final representation of an input G:

$$\mathbf{h}_G = \text{READOUT}(\{\mathbf{a}_u^{(L)} | u \in G\}) \tag{4}$$

where L is the number of GNN layers. The READOUT function should be invariant to permutation, and thus average, sum, and max pooling functions are widely used. The final representation $\mathbf{h}_G$ can then be fed into a trainable component (e.g., a fully connected layer or a linear regressor) to generate the desired predictions.

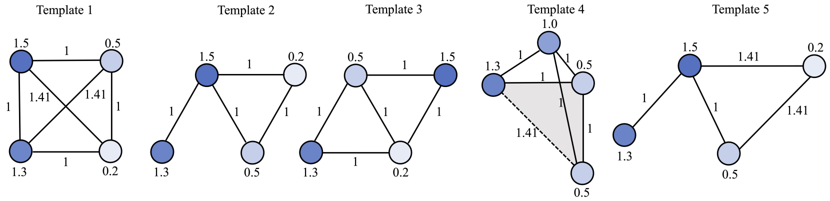

Figure 2: Five templates used to generate the synthetic datasets. Template 2 and 5 are designed to make the classification task more challenging, in which only two edges take different attributes.

Table 1: Graph classification results using synthetic data.

Dataset size	GAT	GCN	GIN	MCL-LR
500	0.691 ± 0.020	0.745 ± 0.033	0.640 ± 0.035	**0.996** $\pm$ **0.008**
10000	0.734 ± 0.028	0.853 ± 0.016	0.749 ± 0.010	**0.997** $\pm$ **0.001**

3 Experiments

We applied MCM to both synthetic and real data to thoroughly evaluate its potential in classifying graphs, predicting graph properties, and learning semantically explainable representations. All experiments use 1-hop neighborhoods in building motifs.

3.1 Classification on the synthetic dataset

This experiment shows the advantage of motif convolution in capturing local structural context over GNNs. We designed 5 ARG templates (Figure 2), and one synthetic dataset of 5 classes, which share similar node attributes but have different structures. This template can only be well distinguished by their overall structures. For example, templates 2 and 5 are very similar to each other except for two edges have different attributes. Sample ARGs were produced from these 5 ARG templates by randomly adding nodes to templates and adding Gaussian noises of $\mathcal{N}(0, 0.1)$ to node attributes. The number of added nodes in each sample ARG was sampled from a binomial distribution $B(4, 0.1)$. Each sample ARG is labeled by the ID of its ARG template. The task is to predict the template ID of any given synthetic ARG. We synthesized two datasets of sizes 500 and 10,000, respectively. Each template contributed to 20% of each dataset.

We only used the MCL of the MCM as it was already sufficient. The readout of the MCL is fed to a logistic regressor (LR) to output the classification result. Standardization was applied to the readout by removing the mean and scaling to unit variance. We named this model MCL-LR. Two readout functions (average pooling and max pooling) were tried, and max pooling always outperformed average pooling. A motif vocabulary of size 5 was constructed. We tried using more than 5 motifs, and found no significant advantage. We compared MCL-LR with several baseline models built from GNN variants with edge weight normalization implemented by Wang et al. (2019), including GCN Kipf & Welling (2017), GIN Xu et al. (2018b) and GAT Veličković et al. (2018) (detailed model configurations in Appendix A.5.2).

We ran each model 20 times on both datasets. In each run, each dataset was randomly split into 8:1:1 for training, validation and test. The average prediction accuracy, as well as the standard deviation, are reported in Table 1. The MCL-LR models significantly outperform other models by an average of 20%. In addition, MCL-LR requires substantially smaller training data as it is able to achieve near-perfect results on the 500 datasets. We observed that the learned motifs were quite similar to the underlying templates (Appendix Figure A.7) and contains necessary local structures for discriminant purpose, which explain the superior performance of MCL-LR. The performance by categories (Appendix Table A.6) suggests that MCL-LR is able to discriminate highly similar templates, as in the case of templates 2 and 5 in the appendix table. In addition, we observed that training of GNNs on the larger dataset took more time and computational resources than MCL-LR.

Table 2: Compare test ROC-AUC (mean ± std) on molecular property prediction benchmarks. The best result for each dataset is in bold.

Dataset	bace	bbbp	clintox	sider	tox21	toxcast	hiv
GCN	0.811 ± 0.030	0.881 ± 0.036	0.615 ± 0.102	0.615 ± 0.025	0.784 ± 0.017	0.633 ± 0.007	0.754 ± 0.067
GIN	0.797 ± 0.049	0.873 ± 0.036	0.530 ± 0.065	0.616 ± 0.025	0.783 ± 0.024	0.634 ± 0.009	0.762 ± 0.058
MICRO-Graph	0.819 ± 0.004	0.870 ± 0.008	0.540 ± 0.024	0.617 ± 0.018	0.774 ± 0.006	0.635 ± 0.006	0.780 ± 0.026
MGSSL (DFS)	0.797 ± 0.008	0.705 ± 0.011	0.797 ± 0.022	0.605 ± 0.007	0.764 ± 0.004	0.638 ± 0.030	0.795 ± 0.011
MGSSL (BFS)	0.791 ± 0.009	0.697 ± 0.001	**0.807** ± **0.021**	0.618 ± 0.008	0.765 ± 0.003	0.641 ± 0.070	0.788 ± 0.012
MCM + GCN	0.806 ± 0.026	**0.917** ± **0.031**	0.612 ± 0.145	0.624 ± 0.024	0.794 ± 0.015	0.650 ± 0.012	0.792 ± 0.046
MCM + GIN	**0.820** ± **0.055**	0.900 ± 0.031	0.655 ± 0.139	**0.627** ± **0.028**	**0.802** ± **0.015**	**0.651** ± **0.010**	**0.800** ± **0.043**

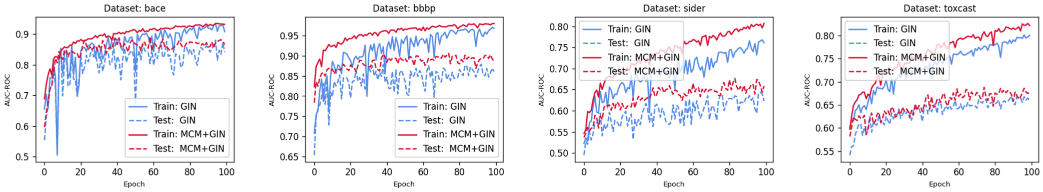

Figure 3: The training and testing curves on molecular benchmarks suggest MCM+GIN converge faster and more stably than GIN.

3.2 Classification on molecular benchmarks

We conducted an experiment using several small and medium sized molecular benchmark datasets in MoleculeNet Wu et al. (2018). We compared our model with MICRO-Graph Subramonian (2021) and MGSSL Zhang et al. (2021) with different generation orders (BFS and DFS), which are also pre-training frameworks for GNNs with a motif-aware fashion. The results demonstrate that MCM can be integrated with GNNs in a broad way. An MCM+GNN model uses the MCM component to preprocess input graphs. We used the open-source package RDKit Landrum (2013) to parse the SMILES formula of molecules and performed scaffold-split Hu et al. (2019); Ramsundar et al. (2019) to get the train-validation-test split as 8:1:1. Following the suggestions in MGSSL Zhang et al. (2021), both baseline models (GIN and GCN) have 5-layer with hidden dimension of 300. Mean pooling is used as the readout function after convolutional layers. Both MCM+GCN and MCM+GIN use a motif vocabulary of size 100. Smaller baseline models (3 conv layers and 64 hidden dim in GCN/GIN) are used in MCM-GCN/GIN on all datasets. For each dataset, we carried out 5 independent runs and reported means and standard deviations. Table 2 shows that GNNs integrated with MCM consistently perform better than the base models. Figure 3 compares the training and test curves of MCM+GIN and GIN, and shows that MCM significantly speeds up and stabilizes training, suggesting MCM+GIN is fundamentally more expressive than GIN. We believe this is because MCM encodes local structural information that is not sufficiently captured with traditional message passing in GNNs. The details of training settings and data preprocessing are provided in Appendix A.5.3.

3.3 Molecule property prediction on QM9

The QM9 dataset Ramakrishnan et al. (2014) is a widely used benchmark for evaluating models that predict quantum molecular properties. It consists of about 130k organic molecules with up to 9 heavy atoms (C, O, N and F). The mean absolute error (MAE) of target properties is the commonly used evaluation metric. We adopted the data-splitting setting used in Klicpera et al. (2020b;a); Zhang et al. (2020). More specifically, following Faber et al. (2017), we removed about 3k molecules that failed the geometric consistency check or were hard to converge. We applied random splitting to the dataset, which takes 110,000 molecules for training, 10,000 for validation, and the rest for test. We only used the atomization energy for U_0, U, H and G, by subtracting the atomic reference energies as in Klicpera et al. (2020b). For property $\Delta\epsilon$, we followed the DFT calculation and calculate it by simply taking $\epsilon_{LUMO} - \epsilon_{HOMO}$.

We designed the MCM to be MCL + 2-layer MLP (MLP: input → 128 → ReLU → 128 → output). The motif vocabulary size is represented as a hyper-parameter, where we tried 100 and 600 in the ex-

Table 3: Comparison of MAEs of targets on QM9 dataset for different tasks.

Task	SchNet	DimeNet	DimeNet++	MXMNet	MXMNet	MCM+MXMNet	MCM+MXMNet
				d_g = 5Å	d_g = 10Å	d_g = 5Å	d_g = 10Å
μ (D)	0.033	0.0286	0.0297	0.0382	0.0255	0.0375	**0.0251**
$\alpha(a_0^3)$	0.235	0.0469	**0.0435**	0.0482	0.0465	0.0477	0.0456
ϵ_{HOMO} (meV)	41	27.8	24.6	23.0	22.8	**21.9**	22.6
ϵ_{LUMO} (meV)	34	19.7	19.5	19.5	18.9	**18.5**	18.6
$\Delta\epsilon$ (meV)	63	34.8	32.6	31.2	**30.6**	32.1	31.9
$\langle R^2 \rangle(a_0^2)$	**0.073**	0.331	0.331	0.506	0.088	0.489	0.124
ZPVE (meV)	1.7	1.29	1.21	1.16	1.19	**1.14**	1.18
U_0 (meV)	14	8.02	6.32	6.10	6.59	**5.97**	6.49
U (meV)	19	7.89	6.28	6.09	6.64	**6.02**	6.51
H (meV)	14	8.11	6.53	6.21	6.67	**6.01**	6.50
G (meV)	14	8.98	7.56	7.30	7.81	**7.13**	7.54
$c_v(\frac{cal}{molK})$	0.033	0.0249	0.0230	**0.0228**	0.0233	0.0230	0.0234

periments. We formed our model MCM+MXMNet by connecting the above MCM to an MXMNet. Two options (5Å and 10Å) were tested for the distance cut-off hyper-parameter d_g of MXMNet. A separate model was trained for each target property and used grid search on learning rate, batch size, motif number, and cut-off distance d_g. Edges in molecules are defined by connecting atoms that lie within the cut-off distance d_g. Following Klicpera et al. (2020b), we did not include auxiliary features like electronegativity of atoms. Detailed training settings are provided in Appendix A.5.4, and the discussion of motif vocabulary construction and efficiency is in Appendix A.5.5.

We compared our model MCM+MXMNet with several other state-of-the-art models including SchNet Schütt et al. (2017), DimeNet Klicpera et al. (2020b), DimeNet++ Klicpera et al. (2020a) and MXMNet Zhang et al. (2020). For other models, we use the results reported in their original works. All experiments were run on one NVIDIA Tesla V100 GPU (32 GB). Table 3 summarizes the comparison results, and shows that our model MCM+MXMNet outperforms others on eight molecule property prediction tasks. For two MXMNet settings, a larger cut-off distance (i.e., d_g = 10Å) can lead to better results for some tasks, but not all of them. This is because larger d_g leads to a larger receptive field and thus helps to capture longer range interactions. However, higher d_g might cause redundancy or oversmoothing in message passing and will also increase computation cost. We observed a similar phenomenon for MCM+MXMNet. We also observed that under the same d_g setting, MCM+MXMNet tends to perform better than MXMNet. We believe that this is because MCM helps to produce more informative node representations that better encode local chemical context.

3.4 Explainability of motif convolution

The embeddings that MCM learns are highly explainable and encode domain semantics. We visualize the representations of carbons produced by a MCM with 600 motifs in the QM9 experiment. The visualization is done using the T-distributed Stochastic Neighbor Embedding (t-SNE) algorithm Van der Maaten & Hinton (2008). We randomly sampled 15,000 molecules from the QM9 dataset, and then randomly selected 2 carbons from each chosen molecule. Figure 4 shows the t-SNE visualization of these 30,000 atoms' representations learned by MCM. To better understand our representation, we manually labelled 300 carbons randomly sampled from the above 30,000 carbons according to their 1-hop local structures. We observe that carbons in the same local context tend to cluster together and are separated from those in different local structures.

More interestingly, we observe that node representations learned by MCM encode meaningful chemical properties. For example, the carbons (red in Figure 4A) in the Trifluoromethyl (-CF_3) groups are tightly clustered together, actually stacked into one point. It is known that the more fluorines are connected to a carbon, the shorter the bonds from this carbon Peters (1963), which makes the Trifluoromethyl groups very different from other substructures. Moreover, Methylene (-CH_2-) is the most common 'bridge' in organic chemistry, connecting all kinds of functional groups (R, R'). Hence, the carbons (pink in Figure 4A) in the Methylene groups are scattered apart because of their diverse contexts. The carbons in the alcohol functional groups (-CH_2OH, green in Figure 4A) are clustered into two separate sub-groups. This is because they are connected to two very different chemical structures (Figure 4B): cyclic functional groups and linear functional groups.

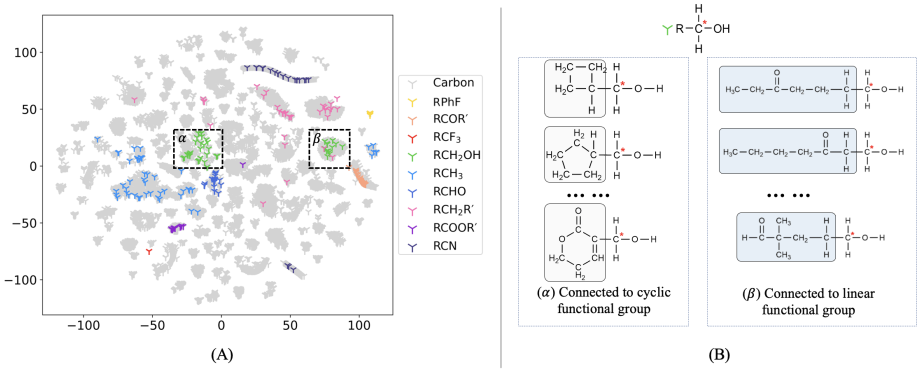

(α) Connected to cyclic functional group

(β) Connected to linear functional group

Figure 4: Node embeddings learned by MCM. **(A)**: The t-SNE visualization of carbon representations learned by MCM. There are 30,000 carbons randomly sampled from the QM9 dataset. Among them, 300 are randomly chosen and are colored based on types of functional groups that carbons belong to, for example, alcohol(-OH) in green, three fluorines (F$_3$) in red, and so on. Both R and R' are the abbreviations for groups in the rest of a molecule. The details of the 9 local structure groups are listed in Table A.7 in Appendix. The green group are separated into two sub-groups (α and β). **(B)**: The carbons, whose representations visualized in the Left, are marked by red *. The carbons in the green group share the same 1-hop local structures shown at the top. The two green sub-groups have distinct characteristics in their at-large local structures. In the α cluster, the marked carbons are connected to cyclic functional groups. In the β cluster, the marked carbons are connected to linear functional groups.

3.5 Efficiency of GPU accelerated motif convolution

The highest workload in MCM comes from matching motifs with subgraphs, which can be sped up tremendously using parallel computing in GPUs. We developed a CUDA-enabled graph matching kernel (Appendix A.3.4) for matching multiple Motif-ARG pairs concurrently, which offer an essential boost to this work. We tested the efficiency of our graph matching kernel under various settings. All experiments were run on NVIDIA GeForce RTX 2080 11GB GPUs. We created 4 test datasets with graph sizes of 10, 15, 20, and 25, respectively. Each set contains 500 molecules sampled from the QM9 dataset. We ran our CUDA-enabled graph matching kernel using up to 8 GPUs to compute pair-wise matching within each dataset. In total, there are 124,750 pairs. The execution times (including loading data from hard disks) of different settings are compared in Figure 5. In general, as expected, it took longer to match larger ARGs. More GPUs help to accelerate the computation. When using # GPUs ≤ 4, doubling GPU devices approximately reduced the execution time by half, which indicates that our kernel achieved a balanced workload in parallel. Using more than 5 GPUs only offered marginal speed improvements because GPUs spent significant amounts of time waiting for data to be loaded.

4 Related works

Early graph embedding methods Perozzi et al. (2014); Tang et al. (2015); Grover & Leskovec (2016) preserve local neighborhoods of nodes by using biased random-walk based objectives. Some other works, such as Sun et al. (2019); Velickovic et al. (2019); Peng et al. (2020), train node encoders by maximizing the mutual information between local and global representations. These methods encourage the preservation of vertex proximity (i.e., nearby nodes to have similar embeddings) and were originally designed and evaluated for node- and edge-level predictions. However, such methods do not work well for predicting graph-level properties (e.g., molecular properties) since they over-emphasize vertex proximity at the expense of global structural information. For instance, random-walk based methods Perozzi et al. (2014); Tang et al. (2015); Grover & Leskovec (2016) consider limited substructures (e.g. subtrees) as graph representatives. There are several other efforts Henderson et al. (2012); Narayanan et al. (2016); Ribeiro et al. (2017) for capturing the structural identity of nodes. However, the applications of such approaches are limited because of their rigid notions of structural equivalence.

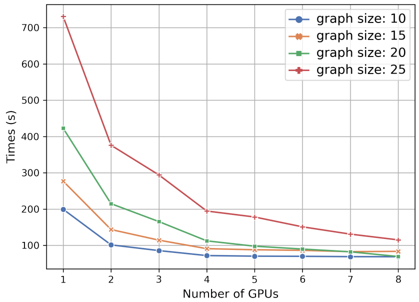

Figure 5: Test speed of pair-wise matching on GPUs. Each dataset contains 500 molecular graphs.

Recently, self-supervised approaches were proposed for pre-training GNNs Hu et al. (2019; 2020); You et al. (2020b); Rong et al. (2020); Sun et al. (2020); Qiu et al. (2020); Hafidi et al. (2020); Hassani & Khasahmadi (2020); You et al. (2020a); Xu et al. (2021); Subramonian (2021); Zhao et al. (2021). Self-supervised tasks at node-, edge- and graph-levels were carefully designed to learn general structural and semantic representations that can be fine-tuned for downstream tasks. These approaches broadly fall into two categories. The first one trains models to predict randomly masked out node attributes Hu et al. (2019) or subgraphs Hu et al. (2020). The second one adopts contrastive learning to maximize representation consistency under perturbations You et al. (2020a); Subramonian (2021); Hassani & Khasahmadi (2020); Zhao et al. (2021). However, these approaches cannot capture the rich information in subgraphs or graph motifs. A few works have been reported to leverage motif-level information. For example, early works like Narayanan et al. (2016); Henderson et al. (2012) encode local structures as binary properties, which do not reflect deformations of local structures that can happen naturally. Domain knowledge is used to extract motifs and treat them as identifiers Rong et al. (2020). MICRO-Graph Subramonian (2021) is a motif-driven contrastive learning approach for pretraining GNNs in a self-supervised manner. MGSSL Zhang et al. (2021) incorporates motif generation into self-supervised pre-learning for GNNs. There is much room for improvements to take advantages of local structural information and produce highly explainable node representations. The challenge in motif-based approaches mainly comes from the difficulty in efficiently measuring similarities between input graphs and the automatic construction of a high quality motif vocabulary.

Our work is related to graph kernel methods that utilize local structures to enhance graph representation. Detailed discussions are presented in Appendix A.4.

5 CONCLUSIONS

This work presents MCM, a novel motif-based representation learning technique that can better utilize local structural information to learn highly explainable representations of ARG data. To our best knowledge, this is the first motif-based learning framework targeting graphs that contain both node attributes and edge attributes. MCM first takes motif discovery from a dataset and applies motif convolution to extract initial context-aware representations for the nodes in input ARGs, which are then embedded in higher level representations using neural network learning. To leverage the power of existing GNNs and target particular applications (e.g., graph classification or regression applications), MCM can be connected as a preceding component to any GNN. One key computational step in MCM is matching ARGs, which is NP-hard in theory and has sub-optimal solutions. To make it possible to apply MCM to large-scale graph datasets, we modified a graduated assignment algorithm for matching ARGs and implemented a CUDA-enabled version. We show that our approach achieves better results than the state-of-the-art models in a graph classification task and a challenging large-scale quantum chemical property prediction task. Moreover, experimental results highlight the ability of MCM to learn context-aware explainable representations. Motif convolution offers a new avenue for developing new motif-based graph representation learning techniques. Currently, the motifs in a MCM are fixed once constructed. In our future work, we will develop motifs that are co-trainable with the rest of a model.

REFERENCES

H.G. Barrow and R.J. Popplestone. Relational descriptions in picture processing. *Machine Intelligence*, 6:377–396, 1971.

Igor I Baskin, Vladimir A Palyulin, and Nikolai S Zefirov. A neural device for searching direct correlations between structures and properties of chemical compounds. *Journal of chemical information and computer sciences*, 37(4):715–721, 1997.

Joan Bruna, Wojciech Zaremba, Arthur Szlam, and Yann LeCun. Spectral networks and locally connected networks on graphs. In *Proceedings of International Conference on Learning Representations*, 2014.

J. Chang, J. Gu, L. Wang, G. Meng, S. Xiang, and C. Pan. Structure-aware convolutional neural networks. In *Neural Information Processing Systems*, 2018.

M. B. Chang, T. Ullman, A. Torralba, and J. B. Tenenbaum. A compositional object-based approach to learning physical dynamics. In *International Conference on Learning Representations*, 2017.

Jianwen Chen, Shuangjia Zheng, Ying Song, Jiahua Rao, and Yuedong Yang. Learning attributed graph representation with communicative message passing transformer. In Zhi-Hua Zhou (ed.), *Proceedings of the Thirtieth International Joint Conference on Artificial Intelligence, IJCAI-21*, pp. 2242–2248. International Joint Conferences on Artificial Intelligence Organization, 8 2021. Main Track.

Luca Cosmo, Giorgia Minello, Michael Bronstein, Emanuele Rodolà, Luca Rossi, and Andrea Torsello. Graph kernel neural networks. *arXiv preprint arXiv:2112.07436*, 2021.

Michaël Defferrard, Xavier Bresson, and Pierre Vandergheynst. Convolutional neural networks on graphs with fast localized spectral filtering. In *Advances in Neural Information Processing Systems*, pp. 3844–3852, 2016. URL https://arxiv.org/pdf/1606.09375.pdf.

Janez Demšar, Tomaž Curk, Aleš Erjavec, Črt Gorup, Tomaž Hočevar, Mitar Milutinovič, Martin Možina, Matija Polajnar, Marko Toplak, Anže Starič, Miha Štajdohar, Lan Umek, Lan Žagar, Jure Žbontar, Marinka Žitnik, and Blaž Zupan. Orange: Data mining toolbox in python. *Journal of Machine Learning Research*, 14:2349–2353, 2013. URL http://jmlr.org/papers/v14/demsar13a.html.

David K Duvenaud, Dougal Maclaurin, Jorge Iparraguirre, Rafael Bombarell, Timothy Hirzel, Alán Aspuru-Guzik, and Ryan P Adams. Convolutional networks on graphs for learning molecular fingerprints. In *Advances in Neural Information Processing Systems*, pp. 2224–2232, 2015.

Felix A Faber, Luke Hutchison, Bing Huang, Justin Gilmer, Samuel S Schoenholz, George E Dahl, Oriol Vinyals, Steven Kearnes, Patrick F Riley, and O Anatole Von Lilienfeld. Prediction errors of molecular machine learning models lower than hybrid dft error. *Journal of chemical theory and computation*, 13(11):5255–5264, 2017.

Aosong Feng, Chenyu You, Shiqiang Wang, and Leandros Tassiulas. Kergnns: Interpretable graph neural networks with graph kernels. *Proceedings of the AAAI Conference on Artificial Intelligence*, 36(6):6614–6622, Jun. 2022. doi: 10.1609/aaai.v36i6.20615. URL https://ojs.aaai.org/index.php/AAAI/article/view/20615.

Thomas Gärtner, Peter Flach, and Stefan Wrobel. On graph kernels: Hardness results and efficient alternatives. In *Learning theory and kernel machines*, pp. 129–143. Springer, 2003.

J. Gilmer, S. Schoenholz, P. F. Riley, O. Vinyals, and G. Dahl. Neural message passing for quantum chemistry. In *International Conference on Machine Learning*, 2017a.

Justin Gilmer, Samuel S Schoenholz, Patrick F Riley, Oriol Vinyals, and George E Dahl. Neural message passing for quantum chemistry. In *International conference on machine learning*, pp. 1263–1272, 2017b.

Steven Gold and Anand Rangarajan. A graduated assignment algorithm for graph matching. *IEEE Transactions on pattern analysis and machine intelligence*, 18(4):377–388, 1996.

M. Gori, G. Monfardini, and F. Scarselli. A new model for learning in graph domains. In *Proceedings of the IEEE International Joint Conference on Neural Networks*, pp. 729–734, 2005.

Aditya Grover and Jure Leskovec. node2vec: Scalable feature learning for networks. In *KDD: proceedings. International Conference on Knowledge Discovery & Data Mining*, volume 2016, pp. 855–864, 2016.

Hakim Hafidi, Mounir Ghogho, Philippe Ciblat, and Ananthram Swami. Graphcl: Contrastive self-supervised learning of graph representations. *arXiv preprint arXiv:2007.08025*, 2020.

Mark Harris. Optimizing cuda. *SC07: High Performance Computing With CUDA*, 60, 2007.

Kaveh Hassani and Amir Hosein Khasahmadi. Contrastive multi-view representation learning on graphs. In *International Conference on Machine Learning*, pp. 4116–4126. PMLR, 2020.

Mikael Henaff, Joan Bruna, and Yann LeCun. Deep convolutional networks on graph-structured data. *CoRR*, abs/1506.05163, 2015. URL `http://arxiv.org/abs/1506.05163`.

Keith Henderson, Brian Gallagher, Tina Eliassi-Rad, Hanghang Tong, Sugato Basu, Leman Akoglu, Danai Koutra, Christos Faloutsos, and Lei Li. Rolx: structural role extraction & mining in large graphs. In *Proceedings of the 18th ACM SIGKDD international conference on Knowledge discovery and data mining*, pp. 1231–1239, 2012.

Weihua Hu, Bowen Liu, Joseph Gomes, Marinka Zitnik, Percy Liang, Vijay Pande, and Jure Leskovec. Strategies for pre-training graph neural networks. In *International Conference on Learning Representations*, 2019.

Ziniu Hu, Yuxiao Dong, Kuansan Wang, Kai-Wei Chang, and Yizhou Sun. Gpt-gnn: Generative pre-training of graph neural networks. In *Proceedings of the 26th ACM SIGKDD International Conference on Knowledge Discovery & Data Mining*, pp. 1857–1867, 2020.

Fredrik D Johansson and Devdatt Dubhashi. Learning with similarity functions on graphs using matchings of geometric embeddings. In *Proceedings of the 21th ACM SIGKDD International Conference on Knowledge Discovery and Data Mining*, pp. 467–476, 2015.

Stephen C Johnson. Hierarchical clustering schemes. *Psychometrika*, 32(3):241–254, 1967.

Thomas N. Kipf and Max Welling. Semi-supervised classification with graph convolutional networks. 2017.

Johannes Klicpera, Shankari Giri, Johannes T Margraf, and Stephan Günnemann. Fast and uncertainty-aware directional message passing for non-equilibrium molecules. In *Machine Learning for Molecules Workshop, Neural Information Processing Systems*, 2020a.

Johannes Klicpera, Janek Groß, and Stephan Günnemann. Directional message passing for molecular graphs. In *International Conference on Learning Representations*, 2020b.

Greg Landrum. Rdkit documentation. *Release*, 1(1-79):4, 2013.

Eugene L Lawler. The quadratic assignment problem. *Management science*, 9(4):586–599, 1963.

Y. LeCun, Y. Bengio, and G. Hinton. Deep learning. *Nature*, 521:436–444, 2015.

Y. Li, D. Tarlow, M. Brockschmidt, and R. Zemel. Gated graph sequence neural networks. In *International Conference on Learning Representations*, 2016.

Sangrak Lim and Yong Oh Lee. Predicting chemical properties using self-attention multi-task learning based on smiles representation. In *2020 25th International Conference on Pattern Recognition (ICPR)*, pp. 3146–3153. IEEE, 2021.

Chengqiang Lu, Qi Liu, Chao Wang, Zhenya Huang, Peize Lin, and Lixin He. Molecular property prediction: A multilevel quantum interactions modeling perspective. In *Proceedings of the AAAI Conference on Artificial Intelligence*, volume 33, pp. 1052–1060, 2019.

Joseph Menke and Allen Y Yang. Graduated assignment graph matching for realtime matching of image wireframes. In *2020 IEEE/RSJ International Conference on Intelligent Robots and Systems (IROS)*, pp. 5909–5916. IEEE, 2020.

F. Monti, D. Boscaini, J. Masci, E. Rodola, J. Svoboda, and M. M. Bronstein. Geometric deep learning on graphs and manifolds using mixture model cnns. In *IEEE Conference on Computer Vision and Pattern Recognition*, 2017.

Annamalai Narayanan, Mahinthan Chandramohan, Lihui Chen, Yang Liu, and Santhoshkumar Saminathan. subgraph2vec: Learning distributed representations of rooted sub-graphs from large graphs. *arXiv preprint arXiv:1606.08928*, 2016.

Zhen Peng, Wenbing Huang, Minnan Luo, Qinghua Zheng, Yu Rong, Tingyang Xu, and Junzhou Huang. Graph representation learning via graphical mutual information maximization. In *Proceedings of The Web Conference 2020*, pp. 259–270, 2020.

Bryan Perozzi, Rami Al-Rfou, and Steven Skiena. Deepwalk: Online learning of social representations. In *Proceedings of the 20th ACM SIGKDD international conference on Knowledge discovery and data mining*, pp. 701–710, 2014.

David Peters. Problem of the lengths and strengths of carbon—fluorine bonds. *The Journal of Chemical Physics*, 38(2):561–563, 1963.

Jiezhong Qiu, Qibin Chen, Yuxiao Dong, Jing Zhang, Hongxia Yang, Ming Ding, Kuansan Wang, and Jie Tang. Gcc: Graph contrastive coding for graph neural network pre-training. In *Proceedings of the 26th ACM SIGKDD International Conference on Knowledge Discovery & Data Mining*, pp. 1150–1160, 2020.

Raghunathan Ramakrishnan, Pavlo O Dral, Matthias Rupp, and O Anatole Von Lilienfeld. Quantum chemistry structures and properties of 134 kilo molecules. *Scientific data*, 1(1):1–7, 2014.

Bharath Ramsundar, Peter Eastman, Patrick Walters, and Vijay Pande. *Deep learning for the life sciences: applying deep learning to genomics, microscopy, drug discovery, and more*. O'Reilly Media, 2019.

Leonardo FR Ribeiro, Pedro HP Saverese, and Daniel R Figueiredo. struc2vec: Learning node representations from structural identity. In *Proceedings of the 23rd ACM SIGKDD international conference on knowledge discovery and data mining*, pp. 385–394, 2017.

Yu Rong, Yatao Bian, Tingyang Xu, Weiyang Xie, Ying Wei, Wenbing Huang, and Junzhou Huang. Self-supervised graph transformer on large-scale molecular data. In *NeurIPS*, 2020.

F. Scarselli, S. L. Yong, M. Gori, M. Hagenbuchner, A. C. Tsoi, and M. Maggini. Graph neural networks for ranking web pages. In *Proceedings of the 2005 IEEE/WIC/ACM International Conference on Web Intelligence*, pp. 666–672, 2005.

Kristof T. Schütt, Pieter-Jan Kindermans, Huziel E. Sauceda, Stefan Chmiela, Alexandre Tkatchenko, and Klaus-Robert Müller. Schnet: A continuous-filter convolutional neural network for modeling quantum interactions. 2017.

Nino Shervashidze, SVN Vishwanathan, Tobias Petri, Kurt Mehlhorn, and Karsten Borgwardt. Efficient graphlet kernels for large graph comparison. In *Artificial intelligence and statistics*, pp. 488–495. PMLR, 2009.

Nino Shervashidze, Pascal Schweitzer, Erik Jan Van Leeuwen, Kurt Mehlhorn, and Karsten M Borgwardt. Weisfeiler-lehman graph kernels. *Journal of Machine Learning Research*, 12(9), 2011.

Richard Sinkhorn. A relationship between arbitrary positive matrices and doubly stochastic matrices. *The annals of mathematical statistics*, 35(2):876–879, 1964.

Alessandro Sperduti and Antonina Starita. Supervised neural networks for the classification of structures. *IEEE Transactions on Neural Networks*, 8(3):714–735, 1997.

Teague Sterling and John J Irwin. Zinc 15–ligand discovery for everyone. *Journal of chemical information and modeling*, 55(11):2324–2337, 2015.

Arjun Subramonian. Motif-driven contrastive learning of graph representations. In *Proceedings of the AAAI Conference on Artificial Intelligence*, volume 35, pp. 15980–15981, 2021.

Fan-Yun Sun, Jordan Hoffman, Vikas Verma, and Jian Tang. Infograph: Unsupervised and semi-supervised graph-level representation learning via mutual information maximization. In *International Conference on Learning Representations*, 2019.

Ke Sun, Zhouchen Lin, and Zhanxing Zhu. Multi-stage self-supervised learning for graph convolutional networks on graphs with few labeled nodes. In *Proceedings of the AAAI Conference on Artificial Intelligence*, volume 34, pp. 5892–5899, 2020.

Jian Tang, Meng Qu, Mingzhe Wang, Ming Zhang, Jun Yan, and Qiaozhu Mei. Line: Large-scale information network embedding. In *Proceedings of the 24th international conference on world wide web*, pp. 1067–1077, 2015.

W. H. Tsai and K. S. Fu. Error-correcting isomorphisms of attributed relational graphs for pattern analysis. *IEEE Trans. on Systems, Man, and Cybernetic*, 9(12):757–768, 1979.

Laurens Van der Maaten and Geoffrey Hinton. Visualizing data using t-sne. *Journal of machine learning research*, 9(11), 2008.

P. Velickovic, G. Cucurull, A. Casanova, A. Romero, P. Lio, and Y. Bengio. Graph attention networks. In *International Conference on Learning Representations*, 2018.

Petar Veličković, Guillem Cucurull, Arantxa Casanova, Adriana Romero, Pietro Liò, and Yoshua Bengio. Graph attention networks. In *International Conference on Learning Representations*, 2018.

Petar Velickovic, William Fedus, William L Hamilton, Pietro Liò, Yoshua Bengio, and R Devon Hjelm. Deep graph infomax. *ICLR (Poster)*, 2(3):4, 2019.

AD Walsh. The dependence of the properties of carbonyl compounds upon polarity. *Transactions of the Faraday Society*, 43:158–163, 1947.

Minjie Wang, Da Zheng, Zihao Ye, Quan Gan, Mufei Li, Xiang Song, Jinjing Zhou, Chao Ma, Lingfan Yu, Yujie Gai, Tianjun Xiao, Tong He, George Karypis, Jinyang Li, and Zheng Zhang. Deep graph library: A graph-centric, highly-performant package for graph neural networks. *arXiv: Learning*, 2019.

Boris Weisfeiler and Andrei Leman. The reduction of a graph to canonical form and the algebra which appears therein. *NTI, Series*, 2(9):12–16, 1968.

Zhenqin Wu, Bharath Ramsundar, Evan N Feinberg, Joseph Gomes, Caleb Geniesse, Aneesh S Pappu, Karl Leswing, and Vijay Pande. Moleculenet: a benchmark for molecular machine learning. *Chemical science*, 9(2):513–530, 2018.

K. Xu, C. Li, Y. Tian, T. Sonobe, K. Kawarabayashi, and S. Jegelka. Representation learning on graphs with jumping knowledge networks. In *International Conference on Machine Learning*, 2018a.

Keyulu Xu, Weihua Hu, Jure Leskovec, and Stefanie Jegelka. How powerful are graph neural networks? *International Conference on Learning Representations*, 2018b.

Minghao Xu, Hang Wang, Bingbing Ni, Hongyu Guo, and Jian Tang. Self-supervised graph-level representation learning with local and global structure, 2021. URL `https://openreview.net/forum?id=DAaaaqPv9-q`.

Yuning You, Tianlong Chen, Yongduo Sui, Ting Chen, Zhangyang Wang, and Yang Shen. Graph contrastive learning with augmentations. *Advances in Neural Information Processing Systems*, 33:5812–5823, 2020a.

Yuning You, Tianlong Chen, Zhangyang Wang, and Yang Shen. When does self-supervision help graph convolutional networks? In *International Conference on Machine Learning*, pp. 10871–10880. PMLR, 2020b.

Shuo Zhang, Yang Liu, and Lei Xie. Molecular mechanics-driven graph neural network with multiplex graph for molecular structures. In *Machine Learning for Structural Biology Workshop at the 34th Conference on Neural Information Processing Systems*, 2020.

Zaixi Zhang, Qi Liu, Hao Wang, Chengqiang Lu, and Chee-Kong Lee. Motif-based graph self-supervised learning for molecular property prediction. *Advances in Neural Information Processing Systems*, 34, 2021.

Chengshuai Zhao, Shuai Liu, Feng Huang, Shichao Liu, and Wen Zhang. Csgnn: Contrastive self-supervised graph neural network for molecular interaction prediction. In *Proceedings of the Thirtieth International Joint Conference on Artificial Intelligence, Online*, pp. 19–27, 2021.

A Appendix

A.1 Motif Convolution Module

Here we provide more details of MCM introduced in main text Section 2.3. Figure A.6 illustrates an expanded view of MCM. The convolution operation calculates the structural similarity score between every motif in the motif set $\{\mathcal{M}_i\}_{i=0}^{N}$ and the subgraph centering at each node in the input graph. For each node in the input ARG, the similarities between all motifs and the local structure of the node are concatenated to produce a N-dimension context-aware representation, which encodes the local structural features represented by motifs. The motif feature representation can be further transformed by a trainable multilayer perceptron (MLP) network to produce the final MCM-embedding for the input node. If a user choose to omit the MLP component, the motif feature representation will be the MCM-embedding for the input node. Motifs are obtained via a pre-training process described in Section 2.1. The MLP should be trained with the downstream task.

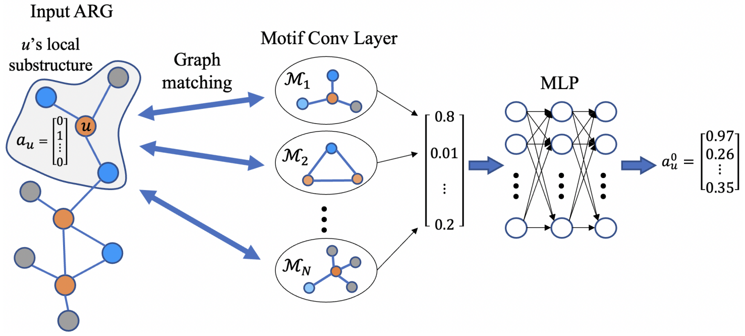

Figure A.6: Motif Convolution Module. The convolution operation computes graph matching between each motif and the local structure centering at each node in the input ARG.

A.2 Proof of Theorem 2.1

Theorem 2.1 *If the compatibility functions $s_1(e_{uv}^{(1)}, e_{ij}^{(2)})$ and $s_2(u,i)$ are well-defined and normalized compatibility metrics, $S(G_1, G_2)$ achieves maximum of 1 if and only if G_1 and G_2 are isomorphic. [proof in Appendix A.2]*

First let's give a formal definition of well-defined and normalized compatibility metric $s(x_1, x_2) \in [0,1]$ in the theorem, where x_1 or x_2 are vectors of the same dimension. It takes maximal value of 1 if and only if $x_1 = x_2$. One example could be $s(x_1, x_2) = \exp(-\frac{||x_1 - x_2||^2}{2})$.

Necessity. The first proof is that if G_1 and G_2 are isomorphic, $S(G_1, G_2)$ achieves maximum of 1. Obviously G_1 and G_2 have the same number of nodes and edges given the isomorphism condition ($n_1 = n_2$ and $l_1 = l_2$) . Without loss of generality we could assume the node ordering in two graphs are the same and the matching matrix $\mathbf{M}$ is the identical matrix $\mathbf{I}$. Otherwise we could find a permutation matrix $\mathbf{P}$ to reorder nodes such that $\mathbf{PM} = \mathbf{I}$. Then let's look at the two parts in computing $S(G_1, G_2)$ from eq. (2)

$$\alpha \frac{\sum_{u=1}^{n_1} \sum_{i=1}^{n_2} \mathbf{M}_{ui} s_2(u,i)}{\sqrt{n_1 \times n_2}} = \frac{\alpha}{n_1} \sum_{i=1}^{n_1} s_2(i,i) = \alpha \tag{A.5}$$

$$\sum_{u=1}^{n_1} \sum_{i=1}^{n_2} \sum_{v=1}^{n_1} \sum_{j=1}^{n_2} \frac{\mathbf{M}_{ui}\mathbf{M}_{vj} s_1(e_{uv}^{(1)}, e_{ij}^{(2)})}{2\sqrt{l_1 \times l_2}} = \sum_{i=1}^{n_1} \sum_{j=1}^{n_1} \frac{s_1(e_{ij}^{(1)}, e_{ij}^{(2)})}{l_1} = 1 \tag{A.6}$$

The last equation holds because the number of edges is l_1 and $s_1(e_{ij}^{(1)}, e_{ij}^{(1)})$ takes 1 if edge e_{ij} exists, otherwise 0.

Thus $S(G_1, G_2) = \frac{1+\alpha}{1+\alpha} = 1$ and we finish this proof.

Sufficiency. Another proof is that suppose $S(G_1, G_2) = 1$, then G_1 and G_2 are isomorphic. We will prove by contradiction.

First let's prove that $S(G_1, G_2) < 1$ if $n_1 \neq n_2$ or $l_1 \neq l_2$. (We assume $n_1 \geq n_2$ without loss of generality.)

Since $\mathbf{M}$ is the hard matching matrix, there is at most one nonzero element (taking value 1) per row and per column, defining an injective function $\phi_{\mathbf{M}}$ such that $\phi_{\mathbf{M}}(i) = u$ if $\mathbf{M}_{ui} = 1$. Thus we have

$$\alpha \frac{\sum_{u=1}^{n_1} \sum_{i=1}^{n_2} \mathbf{M}_{ui} s_2(u,i)}{\sqrt{n_1 \times n_2}} = \alpha \frac{\sum_{i=1}^{n_2} s_2(\phi_{\mathbf{M}}(i), i)}{\sqrt{n_1 \times n_2}} \leq \alpha \frac{n_2}{\sqrt{n_1 \times n_2}} \leq \alpha. \tag{A.7}$$

and

$$\sum_{u=1}^{n_1} \sum_{i=1}^{n_2} \sum_{v=1}^{n_1} \sum_{j=1}^{n_2} \frac{\mathbf{M}_{ui} \mathbf{M}_{vj} s_1(e_{uv}^{(1)}, e_{ij}^{(2)})}{2\sqrt{l_1 \times l_2}} = \frac{\sum_{i=1}^{n_2} \sum_{j=1}^{n_2} s_1(e_{\phi_{\mathbf{M}}(i)\phi_{\mathbf{M}}(j)}^{(1)}, e_{ij}^{(2)})}{2\sqrt{l_1 \times l_2}} \leq \frac{2\min(l_1, l_2)}{2\sqrt{l_1 \times l_2}} \leq 1. \tag{A.8}$$

where the first inequality holds because $s_1(e_{\phi_{\mathbf{M}}(i)\phi_{\mathbf{M}}(j)}^{(1)}, e_{ij}^{(2)})$ takes maximum of 1 given edge $e_{\phi_{\mathbf{M}}(i)\phi_{\mathbf{M}}(j)}^{(1)}$ in G_1 is identical to edge $e_{ij}^{(2)}$ in G_2 and takes 0 if either edge not exists, thus there are at most $2\min(l_1, l_2)$ nonzero terms in the summation.

Strict inequality in the last line of eq. (A.7) holds if $n_1 \neq n_2$ and strict inequality in the last line of eq. (A.8) holds if $l_1 \neq l_2$. Thus $S(G_1, G_2) < \frac{1+\alpha}{1+\alpha} = 1$ if either $n_1 \neq n_2$ or $l_1 \neq l_2$. Thus we complete the first proof.

Next let's prove G_1 and G_2 are isomorphic by contradiction. Note that we already have $n_1 = n_2$ and $l_1 = l_2$. Without loss of generality let's assume the matching matrix $\mathbf{M}$ is the identical matrix $\mathbf{I}$, otherwise we could introduce a permutation matrix to reorder nodes. Then the injective function $\phi_{\mathbf{M}}(i) = i$ becomes identical mapping.

If G_1 and G_2 are not isomorphic, at least one of the following cases must hold:

Case1. (i-th node in G_1 is not identical to i-th node in G_2) $\exists i \in [1, 2, ..., n_2]$, such that $s_2(i,i) < 1$. Thus eq. (A.7) takes strict inequality.

Case2. (Edge $e_{ij}^{(1)}$ in G_1 is not identical to edge $e_{ij}^{(2)}$ in G_2, or either edge not exists.) $\exists i, j$, such that $s_1(e_{ij}^{(1)}, e_{ij}^{(2)}) < 1$. Thus eq. (A.8) takes strict inequality.

For either case, we obtain the strict inequality and thus $S(G_1, G_2) < \frac{1+\alpha}{1+\alpha} = 1$, which leads to contradiction.

A.3 GPU-enabled ARG Matching.

A.3.1 ARG matching used in MCM

The convolution operation calculates the structural similarity score between the motif M_i from Motif Conv Layer and u's local substructure from the input ARG. Before taking convolution, we should find the optimal matching assignment between M_i and u's local subgraph. Graph matching problem is NP-hard that has been well-studied for couples of years. In the following section we briefly introduce the problem definition and efficient approximated solutions that proposed by (Gold & Rangarajan, 1996; Menke & Yang, 2020). To make the computation of graph matching more efficient in practice and meets the need of high frequent calculation in MCM, we proposed a CUDA-enabled the methods to accelerate ARG matching, which could achieve 10,000x speed up than running on CPUs.

A.3.2 ARG matching

It should be noted that finding the optimal matching between two ARGs is NP-hard and can be formulated as a Quadratic Assignment Problem (QAP) (Lawler, 1963). Basically, the optimal matching can be found by solving the following optimization problem:

$$\begin{aligned}\max_{\mathbf{M}\,\in\,\mathbf{R}^{n_1\times n_2}} \quad & \frac{1}{2}\sum_{u=1}^{n_1}\sum_{i=1}^{n_2}\sum_{v=1}^{n_1}\sum_{j=1}^{n_2} s_1(e^{(1)}_{uv}, e^{(2)}_{ij})\mathbf{M}_{ui}\mathbf{M}_{vj} + \alpha\sum_{u=1}^{n_1}\sum_{i=1}^{n_2} s_2(u,i)\mathbf{M}_{ui}, \\ & \text{s.t. } \forall u \sum_{i=1}^{n_2}\mathbf{M}_{ui} \leq 1, \forall i \sum_{u=1}^{n_1}\mathbf{M}_{ui} \leq 1, \forall u, i \; \mathbf{M}_{ui} \in \{0,1\}\end{aligned} \tag{A.9}$$

where $s_1(e_{uv}, e_{ij})$, $s_2(u,i)$, and α are the same to the ones in eq. (2) in the main body. A graduated assignment based algorithm was proposed in Gold & Rangarajan (1996) for finding a sub-optimal matching solutions between two ARGs. A simplified verion of this algorithm was proposed in Menke & Yang (2020) that runs much faster with little compromise in accuracy. Nevertheless, the matching matrix solved by Menke & Yang (2020) does not always fulfill the constraints in eq. (A.9) in the main body, and may produce ambiguous matching results. We develop a greedy iterative method that converts the soft matching matrix $\mathbf{M}$ into a hard matching matrix (i.e., containing binary values). Our method finds the maximum in $\mathbf{M}$, set it to 1, and set all other elements in the same row and column to 0. This step is applied to the rest of $\mathbf{M}$ until the sum of every row/column in $\mathbf{M}$ is at most 1.

The above graph matching algorithm still incurs a substantial computational cost when applied to large-scale graph datasets (e.g., the QM9 dataset). We therefore implemented a version accelerated by GPU computing, which makes it possible for us to apply MCM to large-scale datasets. The efficiency of our GPU-enabled ARG matching algorithm has been discussed in Section 3.5.

A.3.3 Simplified graduated assignment algorithm for ARG matching.

The graduated assignment algorithm Gold & Rangarajan (1996) find sub-optimal graph matching solutions by iteratively solving the first-order Taylor expansion of QAP (eq. A.9). A simplified graduated assignment algorithm was later proposed by Menke & Yang (2020) (pseudo codes included in Algorithm A.1). It first finds the soft assignment matrix that relaxes the constraint $\mathbf{M}_{ai} \in \{0,1\}$ to lie in the continuous range $[0,1]$, then convert it into hard assignment in a greedy way. Algorithm A.1 shows the iteration steps to obtain the approximated assignment matrix. Given the initialization of $\mathbf{M}^0$, the objective function $E(\mathbf{M})$ in Equation A.9 can be approximated via a Taylor expansion at $\mathbf{M}^0$, thus the original optimization problem is equivalent to the assignment problem that maximizes $\sum_{a=1}^{n_1}\sum_{i=1}^{n_2}\mathbf{Q}_{ai}\mathbf{M}_{ai}$, where $\mathbf{Q}_{ai} = \frac{\partial E(\mathbf{M})}{\partial \mathbf{M}_{ai}}\Big|_{\mathbf{M}=\mathbf{M}^0}$ is the partial derivative. The optimal $\mathbf{M}$ at the current step will substitute back as the new initialization and repeat the Taylor approximation period until convergence.

One efficient way to solve assignment with a constraint (row or column summed up to 1) is by taking softmax with control parameter $\beta > 0$ along with the constrained rows/columns, so that $\mathbf{M} = \text{softmax}(\beta\mathbf{Q})$. Increasing β will push the elements in $\mathbf{M}$ to be either 0 or 1 and result in a hard matching when $\beta \longrightarrow \infty$. However, the assignment problem in ARG matching has two constraints (both row and column summed up to 1). To achieve them, the solver can first take the element-wise exponential operation such that $\mathbf{M}_{ai} = \exp(\beta\mathbf{Q}_{ai})$, and then alternatively normalize the rows and columns until converges to a doubly stochastic matrix (i.e., a soft assignment between two input ARGs) Sinkhorn (1964). We initialize β with β_0, and increases it at a rate β_r at each iteration until $beta$ reaches a threshold β_f. In the end, the soft assignment result $\mathbf{M}$ is converted into a hard assignment by a greedy procedure explained in Appendix A.3.2.

A.3.4 GPU accelerated ARG matching

To handle pair-wise matching, we parallelize the process across GPUs to accelerate matching. We implement Line 5 - 16 in Algorithm A.1 with a custom CUDA kernel to process the matching of multiple molecule pairs concurrently. Specifically, each cooperative thread array (CTA) of GPU is assigned to compute the matching between two molecules. In Algorithm A.1, the computation of partial derivative and exponential are element-wise operations. Therefore, we use the each thread within the CTA to compute one element in the assignment matrix and all threads work cooperatively to normalize the assignment matrix, which takes advantage of different levels of parallelism on GPU. We also implement CUDA kernels for computing node- and edge(relation)- similarity and the

Algorithm A.1 Simplified Graduated Assignment for ARG Matching.

```
Input: $G_1$, $G_2$, $\beta_0$, $\beta_r$, $\beta_f$
Output: Hard assignment matrix $\mathbf{M}^*$
$\beta = \beta_0$                                                        ▷ Initialize $\beta$.
$\mathbf{M}_{ui} = s_1(u, i), \forall u \in G_1, \forall i \in G_2$     ▷ Initialize $\mathbf{M}$.
while $\beta \leq \beta_f$ do
    $\forall u \in G_1, \forall i \in G_2$
    $\mathbf{Q}_{ui} = \frac{1}{2} \sum_{v=1}^{n_1} \sum_{j=1}^{n_2} s_2(e_{uv}, e_{ij}) \mathbf{M}_{vj} + \alpha s_1(u, i)$   ▷ Taking the partial derivative.
    $\mathbf{M}_{ui} = \exp(\beta \mathbf{Q}_{ui})$                      ▷ Element-wise exponential operation.

    $\forall u \in G_1, \forall i \in G_2$
    $\mathbf{M}'_{ui} = \frac{\mathbf{M}_{ui}}{\sum_{j=1}^{n_2} \mathbf{M}_{uj}}$   ▷ Normalize by row.
    $\mathbf{M}_{ui} = \frac{\mathbf{M}'_{ui}}{\sum_{v=1}^{n_1} \mathbf{M}'_{vi}}$  ▷ Normalize by col.

    $\beta = \beta * (1 + \beta_r)$                                      ▷ Increase $\beta$.
return $\mathbf{M}^* \longleftarrow$ greedy_hard_assignment($\mathbf{M}$)
```

greedy hard-assignment calculation procedure, so the whole matching algorithm is offloaded onto GPU.

This implementation scales up to a 10 GPU distribution by a workload partition algorithm, which also alleviates the memory pressure of GPU. The algorithm follows the principals that no communication between two partition is needed and the matching of every partition consists of the whole matching result. In this algorithm, we fetch a batch of molecule first, and assign this batch with other non-overlapped batches in dataset without repeat as different partitions. We perform the matching between molecules from two batches respectively in each partition. If there is no unrepeated non-overlapped batches in the dataset, we perform the matching for every molecule in the batch.

A.3.5 Complexity analysis

In this section, we analyze the computational complexity of the proposed graph matching method from two aspects: (1) the simplified graduated assignment in Algorithm A.1, (2) the GPU accelerated matching algorithm in Section A.3.4.

The graduated assignment approach for matching ARGs has a low order of computational complexity $O(l_1 l_2)$, where l_1 and l_2 are the numbers of edges in the graphs. The theoretical computational analysis is discussed in Gold & Rangarajan (1996); Menke & Yang (2020). Note this complexity depends on both the graph size and the sparsity of graphs, that is, the graduated assignment approach becomes more efficient for pairs of sparser graphs. Another worst case analysis of complexity is $O(n_1^2 n_2^2)$, where n_1 and n_2 represent the numbers of nodes in the graphs. Since $l_1 < n_1^2$ and $l_2 < n_2^2$, the complexity $O(l_1 l_2) << O(n_1^2 n_2^2)$ hold for almost all cases. If two input graphs are both fully connected, the graduated assignment achieves its worst case of complexity, $O(n_1^2 n_2^2)$. In real scenarios, the graph is usually sparse ($l_1 \propto n_1$ and $l_2 \propto n_2$) and the complexity becomes $O(n_1 n_2)$.

In addition, we take advantage of the massive parallelism of GPU to address the challenge of complexity. The worst-case complexity of graph matching in Algorithm A.1 is $O(n_1^2 n_2^2)$. In parallel machines like GPU, we use parallel step complexity to asymptotically describe the number of operations performed by threads. In step s of tree reduction, threads perform $\frac{n_1^2 n_2^2}{s^2}$ independent operations. Therefore, the parallel step complexity is $\mathcal{O}(log(n_1) + log(n_2))$ Harris (2007). Likewise, the matching of all pairs of graphs have similar parallelism strategy. In particular, N graphs requires $\frac{N(N-1)}{2}$ matching operations, so the parallel step complexity is $\mathcal{O}(log(N))$. The overall parallel step complexity for matching N graphs is $\mathcal{O}(log(N)log(n))$, where n is the average number of nodes in graphs. Therefore, the CUDA-enhanced matching time is sublinear to the number of graphs and graph sizes, which aligns with the results shown in Figure 5.

A.4 COMPARSION WITH KERNEL METHODS

The proposed motif convolution module is relevant to some graph kernel approaches. Graph kernel methods are also widely used to solve graph classification problems, however, they offer limited expressiveness in handling graphs with continuous attributes. Most graph kernel approaches Shervashidze et al. (2009; 2011); Johansson & Dubhashi (2015); Cosmo et al. (2021); Feng et al. (2022) can only deal with discrete node attributes and binary connections between nodes. Many of them need to perform isomorphism tests, for example, by using the WL-test Weisfeiler & Leman (1968) and its variants. Although those using information propagation kernels, like random walk kernels Gärtner et al. (2003); Feng et al. (2022), are able to handle continuous node attributes, they do not support edges with continuous attributes. Therefore, most kernel approaches are not able to work on graph learning tasks with 3D geometry, where the graph is equipped with both continuous node- and continuous edge- attributes. One application example is the molecular graphs in quantum chemistry (e.g., the QM9 experiment in this study), where the target property highly relates to the 3D geometrical structures of molecules.

A.5 IMPLEMENTATION DETAILS

A.5.1 SETTINGS OF ARG MATCHING

We used the following settings for the ARG matching Algorithm A.1: $\alpha = 0.7$, $\beta_0 = 1$, $\beta_f = 30$, $\beta_r = 0.075$. The node-wise and edge-wise similarity measurements, $s_1(a_u, a_i)$ and $s_2(e_{uv}, e_{ij})$, are task-specific.

In the synthetic data experiment, we defined

$$s_1(a_u, a_i) = \exp(-||a_u - a_i||_2^2)$$
$$s_1(r_{uv}, r_{ij}) = \exp(-3.14 \cdot ||r_{uv} - r_{ij}||_2^2)$$

In experiments on molecular datasets, similarity measurements should consider atom types and edge types (i.e., bond types). Let $\mathbb{1}_{ui}$ be the indicator for atom types agreement: it takes 1 if atom u and atom i are of the same type, and takes 0 otherwise. Similarly, $\mathbb{1}_{(uv,ij)}$ denotes the indicator for edge types agreement. On datasets bace, bbbp, clintox, sider, tox21, ogb-molhiv and ogb-molpcba, we defined

$$s_1(a_u, a_i) = \mathbb{1}_{ui}$$
$$s_1(r_{uv}, r_{ij}) = \mathbb{1}_{(uv,ij)}$$

On QM9 dataset where geometric information, i.e., 3D coordinates for atoms is equipped, we added bond lengths as edge attributes and the compatibility measurement was designed as

$$s_1(a_u, a_i) = \mathbb{1}_{ui}$$
$$s_1(r_{uv}, r_{ij}) = \mathbb{1}_{(uv,ij)} \cdot \exp(-2||r_{uv} - r_{ij}||_2^2)$$

A.5.2 TRAINING SETTINGS USED IN THE SYNTHETIC DATA EXPERIMENT

The following configurations were applied to all GNN variants. Each baseline model contains two GNN convolutional layers followed by a readout function and then a 3-layer MLP to produce predictions. We used a batch size of 32 for the small dataset (500) and 512 for the large one (10,000). We used the Cross-Entropy loss to train all models and used Adam optimizer with default initial weights implemented in PyTorch. To prevent overfitting we used early stopping on the validation loss. We conducted grid search on learning rate, batch size and hidden dimension in GNNs. The hyperparameters were tuned as the following: (1) learning rate $\in \{0.1, 0.01, 0.001\}$; (2) hidden dimension $\in \{32, 64\}$; (3) readout function $\in \{\text{max}, \text{average}\}$; (4) edge weight normalization $\in \{\text{True}, \text{False}\}$.

A.5.3 EXPERIMENTAL SETTINGS ON MOLECULAR BENCHMARKS

The following configurations were applied to all training tasks on the seven molecular benchmarks. We used batch size of 32 and maximal training epoch of 100. We used Adam optimizer with learning rate of 0.001. All experiments are conducted on one Tesla V100 GPU. Before training, we performed data cleaning to remove certain molecules that failed to pass the sanitizing process in the RDKit or contained abnormal valence of a certain atom as suggested in Chen et al. (2021); Lim & Lee (2021). The detailed dataset statistics are summarized in Table A.4. For two motif-level pretraining frameworks, MICRO-Graph Subramonian (2021) and MGSSL Zhang et al. (2021), they were pretrained on 250k unlabeled molecules sampled from the ZINC15 Sterling & Irwin (2015) database and finetuned on each downstream task. MGSSL did the same experiments so we tried reproduction based on their available code and optimal model settings. MICRO-Graph did not take experiments on the datasets we worked on, so we followed the pretraining and fintuning suggestions in MGSSL in reproduction. We were not able to reproduce the same results of MGSSL reported in Zhang et al. (2021). Hence, we copy MGSSL's reported results instead of our reproductions.

Table A.4: Dataset statistics.

Dataset	**# Graphs**	**# Graphs after cleaning**	**# Tasks**
bace	1513	1513	1
bbbp	2039	1953	1
clintox	1478	1469	2
sider	1427	1295	27
tox21	7831	7774	12
toxcast	8578	7245	617
hiv	41127	41125	1

A.5.4 Training settings of MCM+MXMNet on QM9

To make a fair comparison, we used the same training settings (e.g., training and evaluation data splitting, learning rate initialization/decay/warm-up, exponential moving average of model parameters, etc.) employed in MXMNet Zhang et al. (2020). We also kept the same MXMNet configurations (basis functions and hidden layers) as reported in its original paper. The weights of MCM+MXMNet are initialized using the default method in Pytorch. The Adam optimizer was used with the maximal training epoch as 900 for all experiments. The initial learning rate was set to $1e-3$ or $1e-4$. A linear learning rate warm-up over 1 epoch was used. The learning rate is then decayed exponentially with a ratio of 0.1 every 600 epochs. To evaluate on valid/test data, the model parameters are the exponential moving average of parameters from historical models with a decay rate 0.999. Early stopping based on the validation loss was used to prevent overfitting. The motif vocabulary size in MCM was set to 100 or 600. The MCM only adds a small amount of parameters (see Table A.5).

Table A.5: Model parameters in DimeNet, MXMNet and MXMNet+MCM.

Model	**# Params**
DimeNet	2,100,064
MXMNet	3,674,758
MXMNet+MCM, vocab_size=100	3,703,302
MXMNet+MCM, vocab_size=600	3,767,302

A.5.5 Efficiency of executing MCM on QM9

Building motif vocabulary from subgraphs is the most time consuming part in MCM, especially for large-scale datasets. Hierarchical clustering on a gigantic size of subgraphs is prohibitively expensive. For example, from the QM9 dataset, we obtained 0.5 million 1-hop subgraphs. Many of them turn out to be highly similar to each other up to a 3D transformation (rotation + translation). To give an example, the carbonyl functional group (C=O) is quite common in organic compounds. However, the length of the C=O bond in carbonyl may change depending on its local context Walsh (1947). To remove "redundancy", we applied a hierarchical clustering technique using average linkage Johnson (1967), implemented in the Orange3 library Demšar et al. (2013), to group highly A motif is the most representative subgraph in a cluster, which has the highest total similarity to the rest of subgraphs in the cluster. For large datasets like QM9, there is a huge amount of subgraphs, which makes the clustering analysis prohibitively expensive for us. To make the computation feasible for QM9, we randomly sampled 40 sets of subgraphs. For each subset, we took clustering and chose 1,000 most representative subgraphs. Most “redundant” subgraphs were thus removed and we obtained a merged subgraph set of size 44,000. We repeated the procedure: divided them into 4 subsets, took clustering to get 3,000 subgraphs for each subset and finally got a merged set of size 12,000. Another round of single linkage clustering analysis was applied to the pooled set to find the final 100 or 600 representative subgraphs as the motif vocabulary. We applied the same clustering technique to the 12,000 representative subgraphs into 100 or 600 clusters, and chose one representative subgraph from each cluster as a motif.

To cluster subgraphs using hierarchical clustering, we needed to run a large number of pair-wise matching, which took 4.4 hour for each subset on 8 RTX 2080 GPUs. Without considering the geometric information like dataset ogb-molhiv, the graph matching part takes around 1.5 times faster. After constructing the motif vocabulary of size 100, then it takes around 13 hours to generate the motif matching scores for the whole QM9. Importantly though, the matching step can be parallelized in a very efficient manner, resulting in significantly lowered computation time. Additionally, the motif vocabulary construction and scoring process only needs to be performed once per dataset. Once constructed, the motif vocabulary can be reused without additional computational expenses.

A.6 Additional Results

Figure 2 in the main body illustrate the 5 ARG templated used to generate the synthetic dataset. We observed that MCL was able to learn motifs (Figure A.7) highly resembling the templates (Figure 2) used to generate the synthetic datasets.

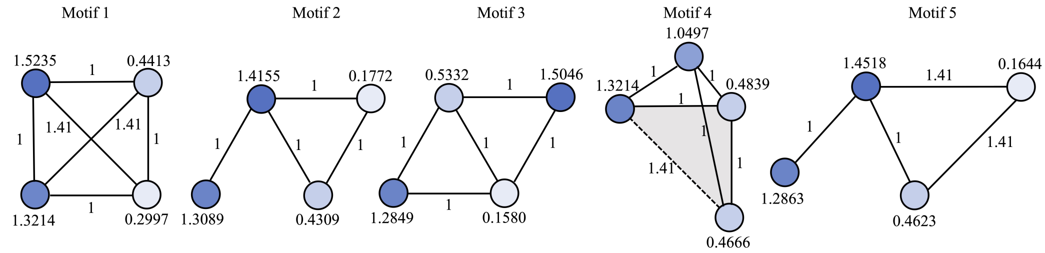

Figure A.7: The motif vocabulary constructed in the synthetic data experiments. The learned motifs resemble the templates (see Figure 2) used to generate the synthetic noisy graphs.

Figure A.8 shows the 3D visualization of several motifs that represent diverse functional groups, including Fluorophenyl, Trifluoromethyl, Nitrile, Aldehyde, Ester and Methyl. The visualizations confirm that the learned motifs are semantically meaningful and make our approach more interpretable.

Table A.6 shows that MCL-LR is especially better than GAT, GCN, and GIN in classifying graphs generated from two similar Templates 2 and 5.

Table A.6: Prediction accuracy for each class on the synthetic dataset.

	Class 1	**Class 2**	**Class 3**	**Class 4**	**Class 5**
GAT	0.710 ± 0.030	0.495 ± 0.112	0.950 ± 0.050	1.000 ± 0.000	0.515 ± 0.096
GCN	0.920 ± 0.014	0.766 ± 0.037	0.857 ± 0.047	0.897 ± 0.024	0.686 ± 0.055
GIN	0.886 ± 0.037	0.296 ± 0.348	0.955 ± 0.017	0.940 ± 0.037	0.668 ± 0.354
MCL-LR	0.996 ± 0.002	0.996 ± 0.004	0.994 ± 0.004	0.998 ± 0.003	0.999 ± 0.001

Table A.7 shows the nine local structure categories of the carbons visualized in Figure 4.

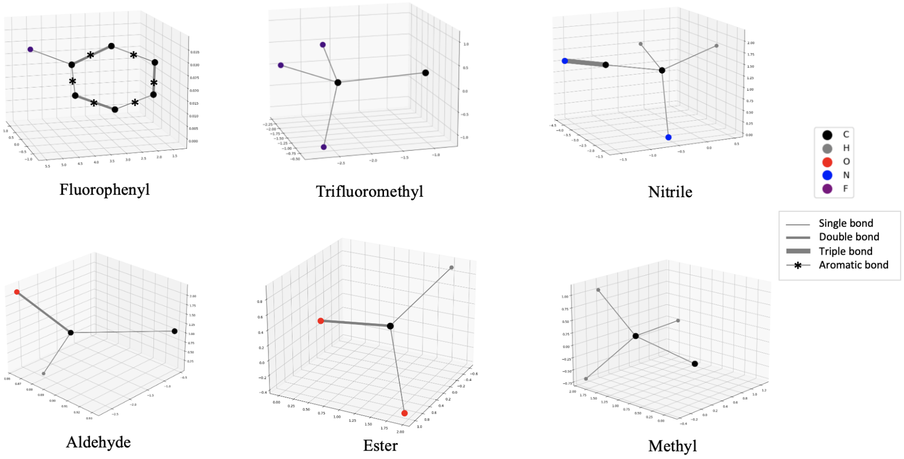

Fluorophenyl

Trifluoromethyl

Nitrile

Aldehyde

Ester

Methyl

Figure A.8: 3D visualization of motifs and the functional groups they represent.

Table A.7: The first column lists the structural abbreviations corresponding to the legends in Figure 4. The second column list the corresponding chemical groups. The first column shows the structure formula.

Abbr	Name	Structural Formula
RPhF	Fluorophenyl	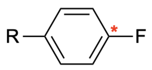
RCF_3	Trifluoromethyl	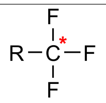
RCH_2OH	Alcohol	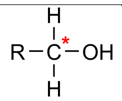
RCHO	Aldehyde	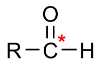
RCOOR’	Ester	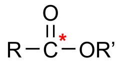
RCOR’	Ketone	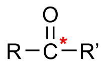
RCN	Nitrile	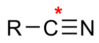
$RCH_2R’$	Methylene	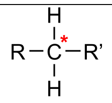
RCH_3	Methyl